Indonesian Journal of Chemical Research

http://ojs3.unpatti.ac.id/index.php/ijcr Indo. J. Chem. Res., 14 (2), 141-152, 2026

Preparation and characterization of a lignocellulosic biosorbent from cocoa pod husks (*Theobroma cacao* L.): optimization by Response Surface Methodology

Sehontinhin Gilles Gouledehi*, David Léonce Kouadio, Kacou Alain Paterne Dalogo, Yapo Hermann Aristide Yapi, Brou Dibi

Laboratoire des Sciences et Technologies de l'Environnement, Université Jean Lorougnon Guédé, BP 150 Daloa, Côte d'Ivoire.

*Corresponding Author: gillesgouledehi@gmail.com

Received: July 2026
Received in revised: August 2026
Accepted: September 2026
Available online: September 2026

Abstract

The valorization of lignocellulosic agro-industrial waste into low-cost adsorbents offers a promising route for treating colored textile effluents. The biosorbent was prepared from cocoa pod husks, an abundant residue in Côte d'Ivoire, through drying, grinding, sieving, and mild alkaline activation without carbonization. The preparation conditions were optimized using design of experiments, with methylene blue removal efficiency as the response—the Plackett-Burman screening of six factors identified particle size and activation temperature as the significant parameters. A central composite design applied to NaOH concentration and activation time yielded a significant quadratic model (R^2 = 95.02 %; F = 26.73; $p < 0.001$), whose optimum (NaOH 0.96 mol L^{-1}, 5 h) predicted a removal efficiency of 96.74%, experimentally confirmed at 92.71% on average, corresponding to an adsorption capacity of about 23.2 mg g^{-1}. Physicochemical characterization (water retention, loss on ignition, FTIR, BET, SEM) confirmed the material's lignocellulosic nature, the persistence of oxygenated surface groups, and a fibrous, lamellar morphology after activation. These results show that alkali-activated cocoa pod husks constitute an effective, economical, and environmentally friendly biosorbent.

Keywords: cocoa pod husk, biosorbent, methylene blue, experimental design, textile effluents, removal efficiency

INTRODUCTION

Access to good-quality water is one of the most pressing environmental and health challenges of our time. The rapid growth of industrial activity has greatly increased pressure on water resources, both through withdrawals and effluent discharges. Among the sectors involved, the textile industry ranks first in water consumption and as a major generator of colored wastewater (Kadhom et al., 2020). Indeed, a substantial fraction of the dyes used during dyeing operations does not fix to the fibers and ends up in the effluents (Nahali et al., 2022). When discharged into receiving environments without prior treatment, these effluents degrade surface-water quality and disrupt aquatic ecosystem balance (Bilal et al., 2022).

Synthetic dyes are highly chemically stable but poorly biodegradable (Khan & Malik, 2018). Even at low concentrations, they impart an intense color to water, reducing light penetration, limiting photosynthesis, and disrupting the entire aquatic food chain (Mansour et al., 2011). Beyond this visual and ecological impact, many dyes are toxic, mutagenic, or even carcinogenic (Zulkania et al., 2020).

Various techniques have been developed to remove dyes from effluents, including biological processes, chemical methods (coagulation-flocculation, advanced oxidation, electrochemical processes) (Tehubijuluw et al., 2023) and physical processes such as membrane filtration and adsorption (Chowdhury et al., 2020; Zaharia et al., 2024). Among them, adsorption stands out as one of the most attractive techniques because of its simplicity of implementation, high efficiency, low cost, and lack of toxic by-products (Bilal et al., 2022). Commercial activated carbon remains the benchmark adsorbent, but its high production and regeneration costs limit its large-scale use, particularly in developing countries, and motivate the search for low-cost alternative adsorbents (Diouf et al., 2026).

In this context, valorizing lignocellulosic agro-industrial waste as precursors for biosorbents is attracting growing interest. Many biomasses have

been successfully investigated for dye removal, including chemically modified bamboo (Guo et al., 2014), fava bean peels (Nahali et al., 2022), banana peels (Susanti et al., 2022), areca nut husks, various agricultural residues (Malik et al., 2016), and husks of *Saba senegalensis* and borassus palm (Diouf et al., 2026).In this context, valorizing lignocellulosic agro-industrial waste as precursors for biosorbents is attracting growing interest. Many biomasses have been successfully investigated for dye removal, including chemically modified bamboo (Guo et al., 2014), fava bean peels (Nahali et al., 2022), banana peels (Susanti et al., 2022), areca nut husks, various agricultural residues (Malik et al., 2016), and husks of *Saba senegalensis* and borassus palm (Diouf et al., 2026).

Chemical activation, whether acidic or basic, further improves the porosity and active-site density of these materials (Jain & Gogate, 2017). Nevertheless, these studies have mostly focused on the adsorption step itself, that is, on the operating parameters governing dye uptake. Meanwhile, the conditions under which the biosorbent is prepared have received far less attention. Yet the preparation stage, through drying, particle size, and the nature and intensity of the chemical activation, directly determines the surface chemistry and the density of active sites of the final material. Researchers rarely optimize this preparation stage systematically, and the interactions among its parameters remain largely unexplored, leaving an open question about the conditions that maximize the performance of a non-carbonized lignocellulosic biosorbent.

Among these biomasses, cocoa pod husks constitute a particularly abundant resource in Côte d'Ivoire, the world's leading cocoa producer (Morales et al., 2025). Bean processing generates large quantities of pods each year, and their husks account for most of the fresh fruit's mass; they are usually left in plantations, where they become breeding grounds for fungal diseases and a source of environmental nuisance (Campos-Vega et al., 2018). Yet this lignocellulosic biomass, rich in cellulose, hemicellulose, lignin, and pectins, has a proven adsorbent potential. Several studies have shown the effectiveness of cocoa pod husks, raw or activated, for pollutant removal (Kouadio et al., 2023; Oussou et al., 2023; Pua et al., 2013). Valorizing them as biosorbents thus fits within a circular economy approach and the sustainable management of local resources.

However, a biosorbent's performance depends closely on its preparation conditions. Conventional optimization using the one-factor-at-a-time (OFAT) method neglects interactions between variables, requires many runs, and does not guarantee a global optimum (Suditu et al., 2022). Design of experiments offers, in this respect, a rigorous and economical alternative, allowing the most influential factors to be screened, the response to be modeled, and the optimal conditions to be identified from a reduced number of experiments (Adjoumani et al., 2019). Combining a Plackett-Burman screening design with a central composite design has proven particularly effective for optimizing adsorption processes (Achour et al., 2021).

Recently, Guerra-Que et al. (2025) valorized NaOH-activated cocoa pod husks for methylene blue removal. However, their study used activated carbon obtained through a carbonization step and applied response surface methodology to the adsorption conditions. More generally, most works on cocoa pod husks either convert the biomass into activated carbon by pyrolysis or optimize the operating parameters of the adsorption step. The originality of the present work lies in two complementary aspects. First, the biosorbent is obtained by a mild alkaline activation, carried out in aqueous phase and at room temperature, without any carbonization step; this soft treatment preserves the lignocellulosic matrix and its oxygenated surface groups (hydroxyl, carbonyl, ether), which are the very sites involved in the binding of cationic dyes, while keeping the process simple and energy-saving. Alkaline activation was preferred because sodium hydroxide exposes cellulose hydroxyl groups and favors negatively charged sites that bind cationic methylene blue, a choice nonetheless assessed experimentally during the screening step (Jain & Gogate, 2017; Pua et al., 2013). Second, a sequential design of experiments strategy, namely a Plackett-Burman screening followed by a central composite design, is applied to the preparation conditions of the biosorbent, and not to the adsorption conditions as is usually done. This combination, aimed at optimizing the synthesis of a non-carbonized cocoa pod husk biosorbent, has not yet been reported for this precursor.

The present work aims to prepare a biosorbent from cocoa pod husks, to optimize its synthesis conditions by design of experiments using the removal efficiency of methylene blue as the response, and to characterize the optimized material by means of complementary physicochemical analyses: water retention capacity, loss on ignition, textural properties by the BET method, Fourier-transform infrared spectroscopy (FTIR), and scanning electron microscopy (SEM). Under the optimized conditions,

the biosorbent achieved high methylene blue removal efficiency, confirming the relevance of the approach for valorizing cocoa pod husks into an effective, low-cost biosorbent.

METHODOLOGY

Materials and Instrumentals

The cocoa pod husks were collected after bean extraction at a plantation in the village of Zépréguhé (about 5 km from Daloa, west-central Côte d'Ivoire), and were free of mold or advanced fermentation. The reagents, of analytical grade (Applichem Panreac, Prolabo, Carlo-Erba, Chem-Lab), included sodium hydroxide (NaOH, 98%), sulfuric acid (H_2SO_4, 95%), hydrochloric acid (HCl, 37%), and methylene blue (a model cationic dye, λ_{max} = 665 nm). The main equipment used consisted of a Memmert oven, a Retsch SK 100 knife mill, a set of sieves (200 µm, 500 µm, 1 mm), a Hanna HI 200M magnetic stirrer, a SIGMA centrifuge, a programmable Nabertherm muffle furnace, a UV-visible spectrophotometer, a Perkin Elmer Spectrum Two FTIR spectrometer (ATR module), and a FEI Quanta 450 scanning electron microscope.

Methods

Preparation of the biosorbent

The biosorbent was prepared in four steps: drying, grinding, sieving, and chemical activation. The husks were first oven-dried at the temperature specified in the experimental design, then manually crushed and ground in a knife mill. The ground material was sieved through 200 µm, 500 µm, and 1 mm meshes, retaining only particles between 0.2 and 1 mm to avoid agglomeration of fine particles and the low specific surface area of coarse particles. Activation was carried out by contacting 20 g of biomass with 200 mL of activating agent, corresponding to a biomass-to-solution ratio of 1:10 (w/v), under magnetic stirring (350 rpm) for a time set by the experimental design. The material was then filtered (Whatman No. 1 paper), washed with distilled water until neutral pH, and oven-dried at 60 °C for 24 h.

Optimization by experimental design

Six preparation factors were first screened using a Plackett-Burman design (Table 1): drying temperature (X1), particle size (X2), type of activating agent (X3), activation time (X4), concentration of the activating agent (X5), and activation temperature (X6). Each Plackett-Burman run was performed in two technical replicates (two full replicates of the design, i.e., 24 runs total), obtained by repeating the adsorption test on the same biosorbent batch. The reported values correspond to the mean of the replicates ± standard deviation, and all 24 runs were used to estimate the experimental error and to perform the analysis of variance. The standard deviation therefore reflects the analytical repeatability of the measurement (weighing, stirring, centrifugation, spectrophotometric determination) rather than the variability associated with material preparation. For the central composite design, five center points ensured repeatability and provided the pure-error estimate used in the lack-of-fit test. The experiment order was not randomized; we carried out the experiments under controlled, constant laboratory conditions, and replication allowed us to estimate experimental error directly.

A central composite design (CCD) was then applied to the two selected factors (NaOH concentration and activation time) in order to model the response and locate the optimum. Design construction and statistical analysis were carried out in Minitab 22.

Table 1. Factors studied and experimental domain of the Plackett-Burman screening design

Variable	Factor	Low level (-1)	High level (+1)
X1	Drying temperature (°C)	35	60
X2	Particle size	φ1	φ2
X3	Type of activating agent	H_2SO_4	NaOH
X4	Activation time (h)	2	4
X5	Concentration ($mol \cdot L^{-1}$)	0.1	0.5
X6	Activation temperature (°C)	26	50

φ1: particles between 0.2 and 0.5 mm; φ2: particles between 0.5 and 1 mm.

The six screening factors were selected based on parameters known to govern lignocellulosic biosorbent preparation and the density of its active sites. The drying temperature (X1) controls moisture and volatile-compound removal but must remain moderate enough to preserve oxygenated surface groups (Jain & Gogate, 2017; Zulkania et al., 2020). Particle size (X2) governs the accessible surface area and the length of the intraparticle diffusion paths, both decisive for biosorption (Güleç et al., 2023). The type

of activating agent (X3) was retained because acidic and alkaline activation modify the material's surface chemistry and porosity differently (Jain & Gogate, 2017; Guo et al., 2014). Activation time (X4) and agent concentration (X5) determine the intensity of the chemical modification: insufficient action limits exposure of active sites, whereas excessive action leads to over-dissolution of the matrix (Guo et al., 2014; Pua et al., 2013). Finally, the activation temperature (X6) affects treatment kinetics but may, at high levels, degrade oxygenated functions and solubilize the hemicellulosic and lignocellulosic fractions (Guo et al., 2014; Jain & Gogate, 2017). The experimental ranges (Table 1) were defined from preliminary trials and ranges reported in the literature to bracket mild activation conditions in the aqueous phase and without carbonization, preserving the lignocellulosic integrity of the precursor.

In a Plackett-Burman design, each factor is studied at two levels, coded -1 and +1. Particle size, an ordinal variable defined by granulometric classes, was handled by assigning the fine fraction to the -1 level and the coarse fraction to the +1 level, each class corresponding to a sieving interval. The type of activating agent, a qualitative variable with two modalities, was introduced as a categorical factor: H_2SO_4 was coded -1 and NaOH +1. For such a factor, the estimated coefficient reflects the contrast between the two modalities rather than a continuous effect, its sign indicating the modality more favorable to the removal efficiency. The domain of the central composite design, defined by the coded levels -α, -1, 0, +1, and +α, is presented in Table 2

Table 2. Coded and actual levels of the central composite design factors

Variable	Factor	$-\alpha$	−1	0	+1	$+\alpha$
X1	NaOH concentration (mol/L)	0.2	0.39	0.85	1.3	1.5
X2	Activation time (h)	2	2.5	4	5.4	6

In total, 13 experiments were performed according to the two-factor CCD matrix. The results were fitted to a second-order polynomial model, allowing evaluation of the linear, quadratic, and interaction effects of the studied factors on the response. The model used is given by Equation (1).

$$Y = \beta_0 + \sum_{i=1}^{k} \beta_i X_i + \sum_{i=1}^{k} \beta_{ii} X_i^2 + \sum_{i<j} \beta_{ij} X_i X_j \quad (1)$$

where Y is the response studied (the methylene blue removal efficiency, RE); β_0 is the model constant; β_i, β_{ii}, and β_{ij} are the linear, quadratic, and interaction coefficients, respectively; and X_i and X_j are the coded variables. The model was evaluated through analysis of variance (ANOVA), the coefficients of determination (R^2 and R^2_{adj}), the Fisher statistic (F), the p-values, the lack-of-fit test, and the mean absolute relative deviation (%D) between experimental and predicted values, defined by Equation (2).

$$\%D = \frac{1}{N} \sum_{1}^{N} \left| \frac{Y_{exp} - Y_{cal}}{Y_{exp}} \right| \times 100 \quad (2)$$

where Y_{exp} and Y_{cal} are the experimental and predicted values of the removal efficiency, respectively, and N is the number of experiments.

The global optimum was determined by analyzing the contour and response surface plots and the desirability function generated by Minitab 22. Finally, control experiments were carried out under the optimal conditions, allowing the experimental and predicted values to be compared. Figure 1 shows the biosorbent obtained.

Figure 1. The prepared biosorbent

Adsorption tests and performance evaluation

All adsorption tests were conducted in batch mode: 0.2 g of material was contacted with 100 mL of a methylene blue solution at 50 mg L^{-1}, under stirring (300 rpm) for 1 h, at room temperature. After centrifugation, the residual concentration was measured by UV-visible spectrophotometry at 665 nm. The removal efficiency RE (%) and the

equilibrium adsorption capacity q_e (mg·g^{-1}) were calculated according to Equations (3) and (4).

$$RE\ (\%) = \frac{(C_0 - C_e)}{C_0} \times 100 \quad (3)$$

$$q_e = \frac{(C_0 - C_e) \times V}{m} \quad (4)$$

where C_0 and C_e (mg L^{-1}) are the initial and equilibrium concentrations, V (L) is the solution volume, and m (g) is the mass of biosorbent. The validity of the models was assessed by analysis of variance (ANOVA), the coefficients of determination (R^2 and R^2_{adj}), the Fisher statistic (F), the p-values, and the lack-of-fit test.

Control tests carried out under the optimal conditions allowed the experimental and predicted values to be compared.

Characterization of the biosorbent

The water retention capacity (WRC) was determined after immersing 2 g of biosorbent in 50 mL of distilled water for 24 h, draining (30 min), and then drying at 105 °C to constant mass, according to Equation (5), where m_0 and m_1 denote the drained wet mass and the dry mass, respectively:

$$WRC\ (g.g^{-1}) = \frac{m_0 - m_1}{m_1} \quad (5)$$

The moisture, dry matter, ash, organic matter (volatile solids, VS), and total organic carbon (TOC) contents were determined by the loss-on-ignition method (Nelson & Sommers, 1996): a fresh mass m_2 is dried at 105 °C to constant mass (m_3, dry mass), then calcined at 600 °C for 4 h (m_4, ash mass). Moisture is expressed on a wet basis, and ash and VS on a dry basis, according to Equations (6) to (9):

$$Moisture\ (\%) = \frac{m_2 - m_3}{m_2} \times 100 \quad (6)$$

$$Ash\ (\%) = \frac{m_4}{m_3} \times 100 \quad (7)$$

$$VS\ (\%) = \frac{m_3 - m_4}{m_3} \times 100 \quad (8)$$

$$TOC\ (\%) = \frac{VS}{1.724} \quad (9)$$

The surface functional groups were identified by FTIR (4000-400 cm^{-1}, ATR module). The morphology was observed by SEM (Low Vacuum mode, backscattered-electron detector). The specific surface area and porosity of the biosorbent were determined by nitrogen adsorption at 77 K using a Micromeritics ASAP 2020 analyzer, following the Brunauer-Emmett-Teller (BET) method. The samples were previously degassed under vacuum at 250 °C for 3 h. The specific surface area was calculated from the adsorption isotherms recorded in the relative pressure range p/p_0 between 0.058 and 0.301.

RESULTS AND DISCUSSION

Screening of factors by the Plackett-Burman design

The Plackett-Burman design is a screening approach that allows the influence of many factors to be evaluated with a limited number of runs, making it a fast and economical way to identify the parameters that most affect the response before any optimization. On this basis, the six preparation factors were screened first. Table 3 presents the results of the Plackett-Burman design, each run being performed in two technical replicates and reported as mean ± standard deviation. The removal efficiencies vary widely from one run to another (29.27 to 95.15%), showing that the preparation conditions influence the performance of the biosorbent (Suditu et al., 2022).

Table 3. Plackett-Burman design matrix

Run	X1	X2	X3	X4	X5	X6	RE (%) ±SD
1	60	φ1	NaOH	2	0.1	26	95.15 ± 0.13
2	60	φ2	H_2SO_4	4	0.1	26	78.14 ± 0.00
3	35	φ2	NaOH	2	0.5	26	84.02 ± 8.80
4	60	φ1	NaOH	4	0.1	50	82.64 ± 4.99
5	60	φ2	H_2SO_4	4	0.5	26	57.98 ± 6.23
6	60	φ2	NaOH	2	0.5	50	40.79 ± 1.11
7	35	φ2	NaOH	4	0.1	50	29.27 ± 4.73
8	35	φ1	NaOH	4	0.5	26	93.73 ± 0.42
9	35	φ1	H_2SO_4	4	0.5	50	79.23 ± 2.94
10	60	φ1	H_2SO_4	2	0.5	50	86.42 ± 5.35
11	35	φ2	H_2SO_4	2	0.1	50	46.84 ± 8.58
12	35	φ1	H_2SO_4	2	0.1	26	86.91 ± 1.41

The coefficients and the p-values associated with each factor studied are presented in Table 4.

Table 4. Coefficients and probability values (p) of the six factors from the Plackett-Burman design

Factors	X1	X2	X3	X4	X5	X6
Coefficient	0.75	-16.57	0.16	-2.58	2.94	-9.89
p-value	0.754	0.000	0.948	0.292	0.232	0.001

The analysis of the coefficients and their associated probabilities (Table 4) identifies the factors that significantly affect removal efficiency. A factor is considered significant when the probability associated with its coefficient is below 0.05 (Adjoumani et al., 2019). On this basis, two factors exert a statistically significant effect: particle size (X2, p = 0.000) and activation temperature (X6, p = 0.001).

The dominant factor is particle size (X2), whose coefficient (-16.57) represents the most pronounced effect in this screening. The negative sign indicates that the low level of the factor leads to a better response, corresponding to the smaller particles (0.2-0.5 mm). This result is explained by a larger accessible surface, a higher density of active sites, and shorter intraparticle diffusion paths, which facilitate biosorption and shorten the equilibrium time (Güleç et al., 2023). Nevertheless, it is advisable not to go below a certain threshold, since overly fine particles tend to agglomerate on contact with water and reduce the effectively available surface; this is why they were discarded during sieving.

The second significant factor is activation temperature (X6), whose negative coefficient (-9.89) indicates that increasing activation temperature decreases the material's performance. A room-temperature activation is therefore preferable. This behavior can be attributed to a partial thermal degradation of certain oxygenated functional groups, such as hydroxyls and carboxyls, that are essential to dye adsorption (Jain & Gogate, 2017). At high temperatures, alkaline hydrolysis also accelerates and causes excessive solubilization of the hemicellulosic and lignocellulosic fractions (Guo et al., 2014), to the detriment of the matrix integrity.

In contrast, the type of activating agent (X3), drying temperature (X1), activation time (X4), and activating agent concentration (X5) show no significant effect within the studied domain. In particular, the very low coefficient for the type of activating agent (0.16) indicates that, under the tested conditions, the acidic or basic nature of the agent does not significantly affect removal efficiency.

Alkaline activation with NaOH was retained for the remainder of the study, as this agent produced the highest removal efficiencies (runs 1 and 8). The drying temperature (X1) was fixed. At the same time, the activation time (X4) and the concentration (X5) were kept for the optimization step: the positive sign of the concentration coefficient (+2.94) suggests a tendency toward improved removal efficiency as the concentration increases, a trend explored more extensively in the central composite design. The effects of these factors may not have been revealed at the tested levels.

Optimization by the central composite design

Once the most influential factors had been identified, the two retained parameters, NaOH concentration and activation time, were studied more thoroughly using a central composite design in order to model the response and locate the optimal preparation conditions.

Table 5 presents the results of the central composite design (CCD) applied to the optimization of the preparation conditions of the cocoa pod husk biosorbent.

Run	Factors		RE (%)	
	X1	X2	Actual	Predicted
1	-1	-1	53.98	57.27
2	1	-1	65.89	62.77
3	-1	1	71.77	70.87
4	1	1	94.97	87.65
5	-1.414	0	55.41	52.88
6	1.414	0	62.08	68.64
7	0	-1.414	65.89	64.92
8	0	1.414	87.14	92.12
9	0	0	92.18	92.54
10	0	0	91.56	92.54
11	0	0	93.16	92.54
12	0	0	94.05	92.54
13	0	0	91.75	92.54

Table 5. Central composite design experimental matrix

The actual values and the model's predictions agree well across the entire experimental domain. The residuals are generally small and randomly distributed around zero, indicating no systematic bias in the model's predictions (Figure 2).

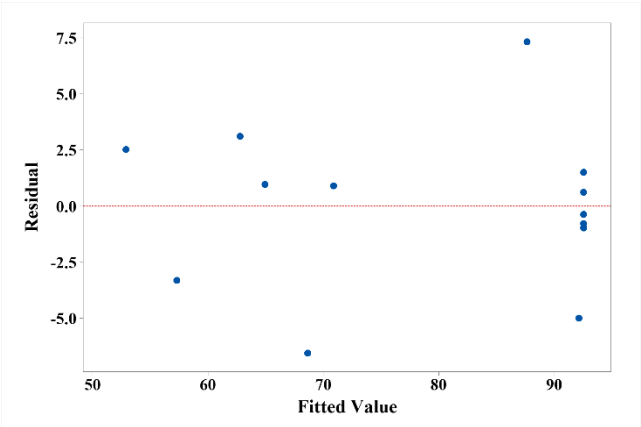

Figure 2. Plot of residuals versus fitted values of the quadratic model from the central composite design

The second-order model generated by Minitab is given by Equation (10).

$$RE = 92.54 + 5.57X_1 + 9.62\,X_2 - 15.89X_1^2 - 7.01X_2^2 + 2.82X_1X_2 \quad (10)$$

where RE represents the theoretical removal efficiency and X1 and X2 are the coded variables of the central composite design (NaOH concentration and activation time, respectively). The statistical data used to evaluate this model are presented in the analysis of variance (ANOVA) in Table 6.

Table 6. Analysis of variance (ANOVA) of the quadratic model from the central composite design

Source	df	Sum of squares	Mean square	F-value	p-value
Model	5	2948.77	589.75	26.73	0.000
Error	7	154.44	22.06		
Lack of fit	3	150.09	50.03	45.93	0.001
Pure error	4	4.36	1.09		
Total	12	3103.21			
Model summary	R^2 = 95.02%; R^2_{adj}=91.47%; R^2_{pred}=65.39%; %D =3.6				

The analysis of variance (Table 6) confirms the statistical significance of the model. The high value of the Fisher test (F = 26.73; p < 0.001) shows that the model captures most of the variation in the response. The model summary gives R^2 = 95.02 %, R^2_{adj} = 91.47 %, and R^2_{pred} = 65.39 %. The high R^2 and R^2_{adj} indicate that the model accounts for most of the variability of the removal efficiency, while the mean absolute relative deviation between experimental and predicted values is low (%D = 3.6 %). The lower R^2_{pred} reflects a more modest ability to predict new observations and is consistent with the significant lack-of-fit discussed below; it indicates that response values predicted outside the tested points should be interpreted with caution. R^2_{pred} nonetheless remains clearly positive, showing that the model retains genuine predictive ability and is suitable for locating the optimum region rather than for precise point prediction.

The residual analysis supports this assessment. The plot of residuals versus fitted values (Figure 2) shows residuals randomly distributed on both sides of zero, with no systematic curvature or funnel-shaped trend that would indicate a gross model inadequacy or marked heteroscedasticity. The five center points, grouped around a fitted value of about 92.5, are tightly clustered near zero, reflecting excellent repeatability at the center of the domain, while the largest residuals correspond to a few individual factorial and axial points, none of which behave as a genuine outlier.

The lack-of-fit is statistically significant (F = 45.93; p = 0.001), but this result must be interpreted with care. The pure error is very low (sum of squares = 4.36) because the center points were highly repeatable; since the replicates were technical, this pure error mainly reflects analytical repeatability rather than variability from material preparation, which makes it particularly small. When experimental variance is this low, even a minor deviation between the model and the data can produce a high lack-of-fit F, making the test hypersensitive to deviations of no practical importance. This significant lack-of-fit, together with the reduced, means that the fitted surface should be regarded as a reliable tool for identifying the region of the optimum rather than as an exact predictor of the response. This optimization is based on the contour plot and the iso-response surface shown in Figure 3.

The contour plot and response surface reveal a well-defined optimum at intermediate NaOH concentrations (0.8 to 1.2 mol L^{-1}) and activation times (4 to 5 h). The elliptical shape of the iso-response lines reflects an interaction between NaOH concentration and activation time, with each effect depending on the level of the other.

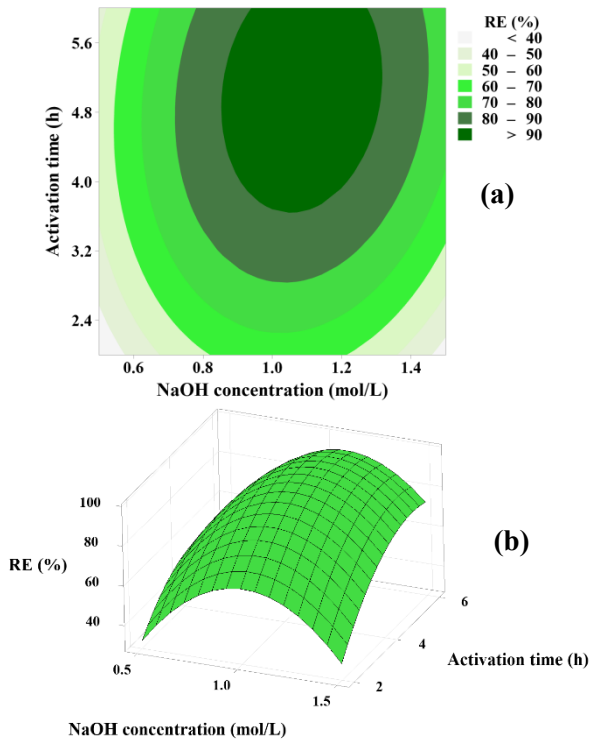

Figure 3. Contour plot **(a)** and response surface **(b)** of the removal efficiency as a function of NaOH concentration and activation time

Mechanistically, alkaline activation saponifies the ester groups of hemicelluloses and partially cleaves lignin bonds, releasing and exposing cellulose hydroxyl groups (Jain & Gogate, 2017). This interpretation is supported by the FTIR analysis of the present material (Figure 5, discussed below), where the shifts of the O-H and C-O/C-O-C bands after activation are consistent with the partial removal of hemicellulose and lignin and the increased exposure of surface hydroxyl groups. At low concentration, longer activation time favors delignification and improves exposure of active sites. At high concentration, by contrast, these reactions are faster and additional time mainly contributes to excessive dissolution of the matrix, to the detriment of performance. The observed optimum thus reflects a compromise between sufficient delignification and preservation of the biosorbent's lignocellulosic integrity, consistent with the performance losses reported for overly harsh alkaline treatments (Guo et al., 2014; Pua et al., 2013). Consequently, process optimization requires a compromise between the intensity of alkaline activation and preserving the biosorbent's chemical integrity. This compromise was determined using the desirability function profile shown in Figure 4.

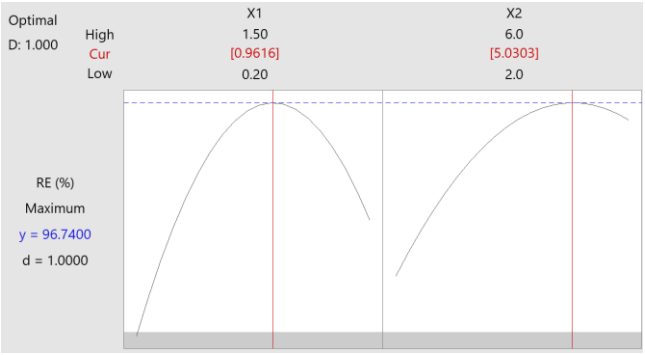

Figure 4. Desirability function profile

This desirability function profile from Minitab first confirms the consistency of the contour and response surface plots. The search for a maximum removal rate yields an overall desirability of 1, indicating optimal attainment of the target response within the experimental domain.

The optimal conditions identified correspond to a NaOH concentration of 0.961 mol L^{-1} and an activation time of 5 h, for which the model predicts a maximum removal rate of 96.74%. Furthermore, the parabolic shape of the individual profiles highlights the system's quadratic behavior, consistent with the ANOVA results. Finally, the optimal removal efficiency, obtained at intermediate factor values, represents a compromise between the effectiveness of alkaline activation and the preservation of the biosorbent's functional groups.

To experimentally verify the model's predictions, additional tests were carried out under the defined optimal conditions; the corresponding removal efficiency and equilibrium adsorption capacity are reported in Table 7.

Table 7. Results of the control tests carried out under the optimal conditions

Run	X1	X2	RE_{cal} (%)	RE_{exp} (%)	q_e (mg g^{-1})	Mean q_e (mg g^{-1})
1	0.96	5	96.74	92.79	23.20	23.18 ± 0.34
2	0.96	5		94.03	23.51	
3	0.96	5		91.31	22.83	

The confirmation tests were carried out under optimal conditions and gave removal efficiencies between 91.31 and 94.03%, with an average of 92.71%. The gap between the predicted value (96.74%) and the mean experimental value corresponds to a relative error of 4.2%, of the same order as the uncertainty of a spectrophotometric measurement. This agreement confirms the model's

validity and the reliability of the determined optimal conditions. Overall, the model should therefore be regarded not as a high-accuracy predictor but as a robust tool for describing the response trends and locating the optimum within the studied domain. Its reliability for optimization rests primarily on the experimental confirmation of the predicted optimum (control tests under optimal conditions, relative error of 4.2 %; Table 7), rather than on the coefficient of determination alone.

Beyond the removal efficiency, the equilibrium adsorption capacity completes the assessment of the material's performance. Under the same optimal conditions, the biosorbent shows a mean experimental capacity of 23.2 mg g^{-1} (23.18 ± 0.34 mg g^{-1}), close to the model-predicted value (24.2 mg g^{-1}). This seemingly moderate capacity must be interpreted in light of the operating conditions: the high biosorbent dosage (2 g L^{-1}) and the relatively low initial methylene blue concentration (50 mg L^{-1}) yield high removal efficiency while mechanically limiting the amount of dye retained per gram of material. A high removal efficiency therefore does not necessarily reflect high adsorption capacity, since q_e depends closely on adsorbent dosage and initial concentration. This single-point value is not directly comparable to the maximum capacities (q_{max}) reported in the literature, which are derived from isotherm studies conducted at higher initial concentrations. Thus, Pua et al. (2013), using a NaOH-treated cocoa pod husk under mild conditions close to ours, reported a q_{max} of 263.9 mg g^{-1}. In contrast, Guerra-Que et al. (2025) obtained about 100 mg g^{-1} for a NaOH-activated cocoa pod husk carbon. Likewise, Latupeirissa et al. (2018) showed that, for a candlenut shell activated carbon, capacity increased with initial concentration (from 23.2 mg g^{-1} at 100 mg L^{-1} to about 47.5 mg g^{-1} at 200 mg L^{-1}). These studies confirm that the retained amount rises markedly with initial concentration and that the material's true potential can be established only through an isotherm study, as noted in the perspectives.

Analysis of surface functional groups by FTIR

To evaluate the effect of alkaline activation on surface functional groups, we also recorded an FTIR spectrum of the raw biomass under the same operating conditions. Figure 5 shows the FTIR spectra of the raw biomass and the NaOH-activated biosorbent.

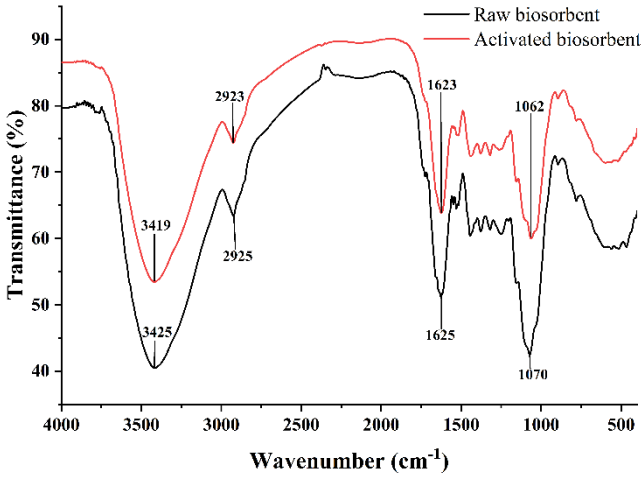

Figure 5. FTIR spectra of the raw biomass and the NaOH-activated cocoa biosorbent

Both spectra display the characteristic absorption bands of lignocellulosic materials, indicating that alkaline activation modified the surface chemistry without destroying the lignocellulosic skeleton. The broad O-H stretching band of cellulose, hemicellulose, and lignin at 3425 cm^{-1} in the raw material shifts to 3419 cm^{-1} after activation, while the C-O/C-O-C band of the polysaccharides shifts from 1070 cm^{-1} to 1062 cm^{-1}. These shifts toward lower wavenumbers reflect changes in the hydrogen-bond network and increased exposure of surface hydroxyl groups, consistent with partial removal of hemicellulose and lignin during alkaline treatment (Jain & Gogate, 2017; Guerra-Que et al., 2025). The aliphatic C-H and carbonyl C=O stretching bands remain almost unchanged, shifting from 2925 to 2923 cm^{-1} and from 1625 to 1623 cm^{-1}; respectively; these 2 cm^{-1} shifts lie within the spectral resolution limit. The persistence of these oxygenated groups (-OH, C=O, C-O-C) after activation favors the binding of cationic methylene blue through electrostatic interactions and hydrogen bonds.

Physicochemical and textural Properties of the biosorbent

The characteristics of the cocoa biosorbent are compiled in Table 8.

Table 8. Physicochemical and textural characteristics of the biosorbent

Characteristics	Values
Water retention capacity (g g^{-1})	0.461 ±0.03
Moisture (%)	11.84 ±0.08
Dry matter (%)	88.16 ±0.08
Ash (%)	11.84 ±0.22
Organic matter / VS (%)	88.16 ±0.022

Total organic carbon (%)	51.15 ±0.07
External surface area (m^2 g^{-1})	36.2
BET specific surface area (m^2 g^{-1})	37.5
Mean pore diameter (nm)	1.9
Total pore volume (cm^3 g^{-1}))	0.018

The water retention capacity of the biosorbent (0.461 g g^{-1}) reflects a moderate hydrophilic character, linked to the presence of cellulose, hemicellulose, and pectins. This hydrophilicity favors the wettability of the material in aqueous medium and the accessibility of the active sites to dye molecules, without leading to excessive swelling that could disrupt the matrix (Ebelegi et al., 2023). The moisture content (11.84%), below 15%, is compatible with good storage stability (Zulkania et al., 2020). The ash content (11.84%) remains comparable to the values reported for cocoa husks (Kouadio et al., 2023). It should be noted that the calcination at 600 °C was performed for analytical purposes only and does not constitute a carbonization step for the biosorbent. Finally, the total organic carbon content (51.15%) confirms the richness of the organic matrix and the potential presence of numerous functional sites involved in adsorption (Anita et al., 2024).

In textural terms, the BET specific surface area of the biosorbent is 37.5 m^2 g^{-1} and is close to the external surface area (36.2), indicating a negligible contribution of microporosity, with the surface being essentially developed by external pores. The mean pore diameter (1.9 nm) and the low total pore volume (0.018 cm^3 g^{-1}) reflect a poorly developed pore network, at the boundary of the mesoporous range. Although moderate compared with commercial activated carbons (500 to 1500 m^2 g^{-1}), this surface area is characteristic of a non-carbonized lignocellulosic material, whose adsorption efficiency relies more on the oxygenated surface functional groups revealed by FTIR than on a high porosity (Nahali et al., 2022; Sukla Baidya & Kumar, 2021).

Surface morphology by SEM

Figure 6 shows the surface morphology of the biosorbent before and after NaOH activation. The SEM micrographs of the raw biosorbent and the NaOH-activated biosorbent are compared in Figure 6. Both samples display a fibrous, lamellar structure typical of lignocellulosic materials, confirming that alkaline activation modifies the surface morphology without destroying the material's architecture. The raw biomass (a) is characterized by a relatively compact, dense surface, whose sheets appear poorly individualized and locally covered with deposits. After activation (b), the surface becomes more irregular and more open: the sheets separate further, revealing a more pronounced relief and more numerous inter-sheet spaces. This evolution is attributed to the NaOH treatment, which removes part of the surface impurities and partially solubilizes lignin and hemicellulose, thereby exposing the fibrous structure of cellulose (Pua et al., 2013). The lamellar appearance and the limited number of open pores are consistent with the low specific surface area and the poorly developed mesoporous network revealed by the BET analysis, with adsorption occurring mainly at the surface and in the inter-sheet spaces.

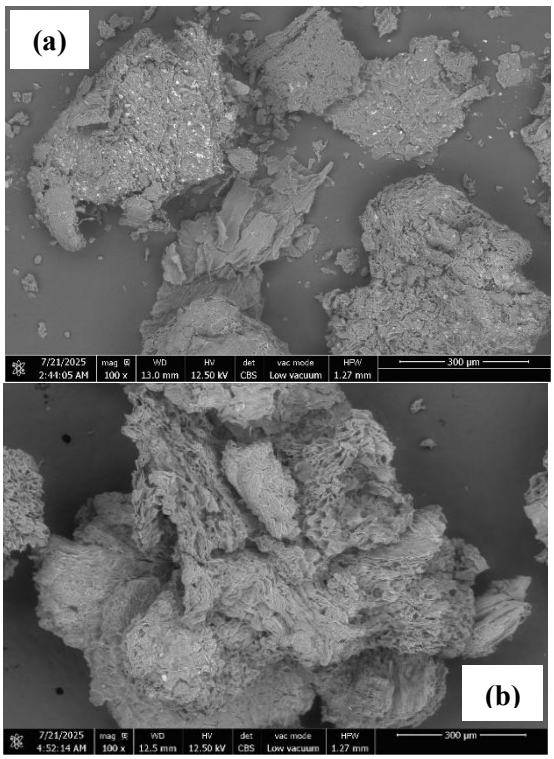

Figure 6. SEM micrographs of the biosorbent: **(a)** raw biomass and **(b)** NaOH-activated biosorbent

CONCLUSION

This study enabled the preparation of a low-cost lignocellulosic biosorbent from cocoa pod husks, an agro-industrial waste abundant in Côte d'Ivoire. Among the six factors screened by the Plackett-Burman design, particle size and activation temperature were the most decisive, fine particles activated with NaOH at room temperature led to the best performance. The central composite design provided a robust quadratic model relating methylene blue removal efficiency to NaOH concentration and activation time, and identified optimal conditions (0.96 mol L^{-1} NaOH, 5 h) that predicted 96.74%

removal efficiency, experimentally confirmed at an average of 92.71%. Physicochemical characterization confirmed the lignocellulosic nature of the material and the persistence of oxygenated surface groups after activation, consistent with a moderate surface area and a fibrous, lamellar morphology favorable for binding cationic dyes. The optimized biosorbent is thus a promising, economical, and environmentally friendly alternative for treating colored textile effluents. Future work will address the in-depth adsorption behavior of the material, including kinetics, isotherms, thermodynamics, the characterization of the dye-biosorbent interactions by FTIR of the methylene blue-loaded material, and its application to real effluents.

ACKNOWLEDGMENT

The authors are grateful to the heads of the Laboratory of Environmental Sciences and Technologies at Jean Lorougnon Guédé University (Daloa, Côte d'Ivoire) for granting access to its facilities and for the support provided throughout this work.

REFERENCES

Achour, Y., Bahsis, L., Ablouh, E.-H., Yazid, H., Laamari, M. R., & Haddad, M. E. (2021). Insight into adsorption mechanism of Congo red dye onto *Bombax buonopozense* bark Activated-carbon using Central composite design and DFT studies. *Surfaces and Interfaces*, *23*, 100977.

Adjoumani, Y. J., Dablé, P. J. M. R., Kouassi, K. E., Gueu, S., Assémian, A. S., & Yao, K. B. (2019). Modeling and Optimization of Two Clays Acidic Activation for Phosphate Ions Removal in Aqueous Solution by Response Surface Methodology. *Journal of Water Resource and Protection*, *11*(02), 200-216.

Anita, S., Hanifah, T. A., Itnawita, I., & Mukhlis, M. (2024). Synthesis, Characterization, and Application of Biosorbent (*Ananas comosus* Morris) Leaves in Reducing the Physical Parameters of Peat Water. *Environment and Ecology Research*, *12*(1), 78-85.

Bilal, M., Ihsanullah, I., Hassan Shah, M. U., Bhaskar Reddy, A. V., & Aminabhavi, T. M. (2022). Recent advances in the removal of dyes from wastewater using low-cost adsorbents. *Journal of Environmental Management*, *321*, 115981.

Campos-Vega, R., Nieto-Figueroa, K. H., & Oomah, B. D. (2018). Cocoa (*Theobroma cacao* L.) pod husk: Renewable source of bioactive compounds. *Trends in Food Science & Technology*, *81*, 172-184.

Chowdhury, M. F., Khandaker, S., Sarker, F., Islam, A., Rahman, M. T., & Awual, Md. R. (2020). Current Treatment Technologies and Mechanisms for Removal of Indigo Carmine Dyes From Wastewater: A review. *Journal of Molecular Liquids*, *318*, 114061.

Diouf, A. L., Diop, S. N., Condé, F., & Cagnon, B. (2026). Elaboration of Activated Carbons from Lignocellulosic Residues (Saba and Palm Tree Husks) for the Adsorption of Ibuprofen. *Chemistry Africa*, *9*(3), 123.

Ebelegi, A., Tonizibeze Elijah, N., & Godwin, J. (2023). Evaluation of Physicochemical Parameters of Biosorbents Produced from Groundnut Hull Using Microwave Assisted Irradiation Method. *Open Journal of Physical Chemistry*, *13*(01), 1-12.

Guerra-Que, Z., López-Margalli, K. S., Urrieta-Saltijeral, J. M., Silahua-Pavón, A. A., Martínez-García, H., García-Alamilla, P., Córdova-Pérez, G. E., Arévalo-Pérez, J. C., & Torres-Torres, J. G. (2025). Activated Carbon Synthesised from Lignocellulosic Cocoa Pod Husk *Via* Alkaline and Acid Treatment For Methylene Blue Adsorption: Optimisation By Response Surface Methodology, Kinetics, And Isotherm Modelling. *RSC Advances*, *15*(55), 47231-47254.

Güleç, F., Williams, O., Samson, A., Kostas, E. T., Stevens, L. A., & Lester, E. (2023). Exploring the Utilisation of Natural Biosorbents for Effective Methylene Blue Removal. *Applied Sciences*, *14*(1), 81.

Guo, J.-Z., Li, B., Liu, L., & Lv, K. (2014). Removal of Methylene Blue from Aqueous Solutions by Chemically Modified Bamboo. *Chemosphere*, *111*, 225-231.

Jain, S. N., & Gogate, P. R. (2017). Adsorptive Removal of Acid Violet 17 dye From Wastewater Using Biosorbent Obtained from NaOH and H_2SO_4 Activation of Fallen Leaves of *Ficus racemosa*. *Journal of Molecular Liquids*, *243*, 132-143.

Kadhom, M., Albayati, N., Alalwan, H., & Al-Furaiji, M. (2020). Removal of Dyes by Agricultural Waste. *Sustainable Chemistry and Pharmacy*, *16*, 100259.

Khan, S., & Malik, A. (2018). Toxicity Evaluation of Textile Effluents and Role of Native Soil Bacterium in Biodegradation of a Textile

Dye. *Environmental Science and Pollution Research*, *25*(5), 4446-4458.

Kouadio, D. L., Yapi, Y. A. H., Meledje, D. E. J. C., Dalogo, K. A. P., Akesse, D. P. V., Dibi, B., & Traore, K. S. (2023). Desorption of Methylene Blue Adsorbed on Activated Carbon from Cocoa Pod Shell. *Open Journal of Applied Sciences*, *13*(05), 605-617.

Latupeirissa, J., Tanasale, M. F. J. D. P., & Musa, S. H. (2018). Kinetika Adsorpsi Zat Warna Metilen Biru Oleh Karbon Aktif dari Kulit Kemiri (*Aleurites moluccana* (L) Willd). *Indonesian Journal of Chemical Research*, 6(1), 12-21.

Malik, D., Jain, C., Yadav, A., Kothari, R., & Pathak, V. (2016). *Removal of methylene blue dye in aqueous solution by agricultural waste*.

Mansour, H. B., Boughzala, O., Dridi, D., Barillier, D., Chekir-Ghedira, L., & Mosrati, R. (2011). Les Colorants Textiles Sources de Contamination de l'eau : criblage de la toxicité et des méthodes de traitement. *Revue des sciences de l'eau*, *24*(3), 209-238.

Morales, S. H. S., Moreno, J. A. J., Contieri, L. S., Rostagno, M. A., & Forster-Carneiro, T. (2025). Cocoa Waste Valorization: A Review and Sustainability Analysis of Green Technologies. *Biofuels, Bioproducts and Biorefining*, *19*(6), 2680-2699.

Nahali, L., Miyah, Y., Mejbar, F., Benjelloun, M., Assila, O., Fahoul, Y., Nenov, V., & Zerrouq, F. (2022). Assessment of Brilliant Green and Eriochrome Black T Dyes Adsorption onto Fava Bean Peels: Kinetics, Isotherms and Regeneration Study. *Desalination and Water Treatment*, *245*, 255-269.

Nelson, D. W., & Sommers, L. E. (1996). Total carbon, organic carbon, and organic matter. In D. L. Sparks, A. L. Page, P. A. Helmke, R. H. Loeppert, P. N. Soltanpour, M. A. Tabatabai, C. T. Johnston, & M. E. Sumner (Eds.), *Methods of Soil Analysis. Part 3: Chemical Methods* (pp. 961-1010).

Oussou, K. F., Guclu, G., Kelebek, H., & Selli, S. (2023). Valorization of Cocoa, Tea and Coffee Processing by-products-wastes. In *Advances in Food and Nutrition Research* (Vol. 107, p. 91-130). Elsevier.

Pua, F. ling, Sajab, M. S., Chia, C. H., Zakaria, S., Rahman, I. A., & Salit, M. S. (2013). Alkaline-treated Cocoa Pod Husk as Adsorbent for Removing Methylene Blue from Aqueous Solutions. *Journal of Environmental Chemical Engineering*, *1*(3), 460-465.

Suditu, G. D., Blaga, A. C., Tataru-Farmus, R.-E., Zaharia, C., & Suteu, D. (2022). Statistical Analysis and Optimization of the Brilliant Red HE-3B Dye Biosorption Onto a Biosorbent Based on Residual Biomass. *Materials*, *15*(20), 7180.

Susanti, I., Iqbal, R. M., Sholeha, N. A., & Putri, K. F. (2022). The Ecofriendly Biosorbent of Methylene Blue Using Banana Peels Waste. *Indonesian Journal of Chemical Research*, *10*(2), 93-96.

Sukla Baidya, K., & Kumar, U. (2021). Adsorption of Brilliant Green Dye from Aqueous Solution onto Chemically Modified Areca Nut Husk. *South African Journal of Chemical Engineering*, *35*, 33-43.

Tehubijuluw, H., Souhoka, F. A., Kusumawati, Y., Prasetyoko, D., Subagyo, R., Nugraha, R. E., & Jalil, A. A. (2023). Characterization and Kinetic Study of Methylene Blue Photocatalytic on ZnO/ZSM-5. *indonesian Journal of Chemical Research.*, *11*(2), 156-162.

Zaharia, C., Musteret, C.-P., & Afrasinei, M.-A. (2024). The Use of Coagulation–Flocculation for Industrial Colored Wastewater Treatment-(I) The Application of Hybrid Materials. *Applied Sciences*, *14*(5), 2184.

Zulkania, A., Iqbal, M., & Syamsumarlin, S. (2020). Characterization of Adsorbents Derived from Palm Fiber Waste and its Potential on Methylene Blue Adsorption. *Key Engineering Materials*, *841*, 273-277.